NASA Technical Memorandum 79095

EFFECTS OF GEOMETRIC AND FLOW-FIELD VARIABLES ON INVERTED-VELOCITY-PROFILE COAXIAL JET NOISE AND SOURCE DISTRIBUTIONS

James R. Stone, Jack H. Goodykoontz
and Orlando A. Gutierrez
Lewis Research Center
Cleveland, Ohio

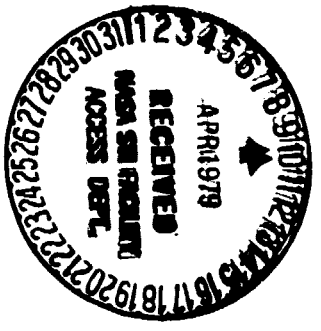

TECHNICAL PAPER to be presented at the
Fifth Aeroacoustics Conference
sponsored by the American Institute of
Aeronautics and Astronautics
Seattle, Washington, March 12-14, 1979

EFFECTS OF GEOMETRIC AND FLOW-FIELD VARIABLES ON INVERTED-VELOCITY-PROFILE COAXIAL JET NOISE AND SOURCE DISTRIBUTIONS

by James R. Stone,* Jack H. Goodykoontz,** and Orlando A. Gutierrez**

National Aeronautics and Space Administration
Lewis Research Center
Cleveland, Ohio 44135

E-9919

ABSTRACT

This paper presents relationships between the noise generation characteristics and the flow-field characteristics for inverted-velocity-profile coaxial jets. Noise measurements were made at four different sideline distances in order to determine the apparent noise source locations, and flow-field characteristics were determined from jet plume pressure/temperature surveys. These relationships are based on a published NASA Lewis prediction model, the basic assumptions of which are shown to be consistent with the experimental data reported herein. Improvements to the noise prediction procedure, on the basis of the present study, are included, which increase the accuracy of the high-frequency noise prediction.

INTRODUCTION

The development of an environmentally and economically acceptable advanced supersonic aircraft will require substantial advancements in noise suppression technology compared to that of the current, first-generation supersonic aircraft. Inverted-velocity-profile coaxial and coannular nozzles have been identified as a major breakthrough in jet noise suppression applicable to supersonic aircraft engines (e.g., ref. 1). The aero/acoustic benefits associated with inverted-velocity-profile jets were first identified in a series of tests under NASA Lewis Research Center sponsorship (refs. 2 to 3). In order to perform noise/cost tradeoff studies for the purpose of identifying the most promising nozzle designs one must be able to relate the noise generation to the flow-field characteristics. The flow-field characteristics must in turn be related to the nozzle geometry and operating conditions. The present paper

*Head, Section A, Jet Acoustics Branch, Member AIAA.
**Aerospace Engineers, Section A, Jet Acoustics Branch.

presents the required relationships, based upon physical principles, which have been obtained from an evaluation of experimental data recently obtained at NASA Lewis Research Center.

It has been recognized (e.g., refs. 4 to 8) that the noise generated by inverted-velocity-profile jets should be modeled as the combined contributions of various independent source regions and noise generation mechanisms. The model presented in this paper is based on that of reference 6 which considers the combined contributions of as many as four uncorrelated constituent sources. Briefly, the model is illustrated in figure 1 and consists of:

(1) Merged-jet/ambient mixing region (subscript m)

(2) Premerged-jet/ambient mixing region (subscript p)

(3) Inner-stream shock/turbulence interaction (subscript s,1)

(4) Outer-stream shock/turbulence interaction (subscript s,2)

The empirical correlations are formulated so that for coplanar jets they approach the single jet case in the limit as the velocities and temperatures, respectively, of the two streams approach equality. The noise from the merged region is relatively low in frequency and is modeled as the contribution from a circular jet at equivalent merged conditions (intermediate between inner and outer streams) and total exhaust area, with the high frequencies attenuated (since the high frequency region of this fictitious jet does not exist). The noise from the premerged region is higher in frequency and is modeled as the contribution of an equivalent plug nozzle at outer stream conditions, with the low frequencies attenuated (since the outer jet is broken up rapidly, before much low frequency noise is generated). The noise prediction models for both jet-mixing regions are those of reference 6, with some improvements to the premerged region model. Reference 6 is, in turn, based on the NASA interim prediction method (ref. 9) for jet mixing noise and a modification of the Harper-Bourne and Fisher (ref. 10) model for shock/turbulence interaction noise.

The prediction method developed in reference 6 was compared with the experimental data available at that time, which covers only a limited range of nozzle geometries. The data presented in this paper and in reference 11 greatly extend the range of geometries. Therefore, comparisons of the prediction with the present data should help validate the prediction over a wider range or identify problem areas wherein the prediction may need improvement.

The prediction model of reference 6 makes use of simplified models for calculating the noise source distributions and jet plume properties. The multiple-sideline noise measurements presented herein are used to develop approximate source location distributions for both the merged and premerged regions. Jet plume surveys are also presented in this paper. These plume surveys and source location data are helpful in assessing the applicability of the simplified methods of reference 6.

APPARATUS AND PROCEDURE

Facility

A photograph of the dual-stream heated-jet facility, described in detail in reference 11, is shown in figure 2. Both streams can provide flows at temperatures from ambient up to ~1100 K and nozzle pressure ratios up to 3.0. Flow rates, total pressures and total temperatures were measured for both streams.

Nozzles

Four different coaxial nozzle configurations were tested in the experimental program, three with coplanar exits and one with a noncoplanar exit. Dimensions of the nozzles are given in figure 3. The area ratios given in the figure are the ratios of the outer nozzle flow area to the inner nozzle flow area. The diameters are the inside diameters of the respective nozzles. Another important geometric parameter given in figure 3 is the ratio of inside to outside radius for the outer stream.

Instrumentation

Acoustic. - Four sideline microphone arrays were used for the tests described herein. Microphones in each array were placed at a constant distance, Y, from the nozzle axis and parallel to the axis, as shown in figure 4. The microphones were placed at the intersection of the sideline with a series of straight lines at a series of angles θ^* to the upstream jet axis. The intersections of those lines with the jet axis correspond to a series of hypothetical point sources related to each far-field angle. This hypothetical source position shifts further downstream with increasing angle, as shown in figure 4. Centerline microphones (i.e., those at the same elevation as the nozzle axis) and ground microphones were incorporated for every measurement angle in each array. The centerline array consisted of eight 0.635-cm condenser microphones with the protective metal grid cap removed to improve the microphone performance at high frequencies. The 1.27-cm ground microphones for the closest array were mounted with diaphragms parallel to the ground, 0.63 cm above a 30-cm square pressed-wood sheet of 0.63 cm thickness. At the larger sideline distances, the ground microphones were mounted with diaphragms perpendicular to the ground and the bottom 0.32 cm off the ground. Each ground microphone was placed at the equivalent acoustic ray location as a corresponding centerline microphone.

Jet plume. - Jet exhaust plume temperature/pressure surveys were made with a proble capable of traversing in the axial direction as well as horizontally and vertically, as illustrated in figure 5. Details of the probe are shown in figure 6. This probe was calibrated in a wind tunnel at subsonic and supersonic speeds. Total temperature, total pressure and static pressure were measured. The plume survey apparatus was removed from the test site during the acoustic tests.

Procedure

Experimental. - Steady-state conditions were attained for each test before the data were recorded. Upstream total temperatures and total pressures for both streams were then automatically recorded, as were the flow-field or acoustic data. For the acoustic tests, the noise signal from each microphone was sequentially analyzed on-line, and 1/3-octave-band sound pressure levels were digitally recorded on magnetic tape for further processing. For the jet plume surveys, probe position, total temperature, total pressure and static pressure were automatically recorded. The traverses were made horizontally at a series of vertical and axial positions.

Jet exhaust conditions. - Ideal nozzle exhaust velocities and Mach numbers were calculated for both streams from the measured upstream temperatures and pressures, assuming complete expansion to atmospheric conditions. The static temperatures were computed from the measured total temperatures after correcting the total temperature measurements for radiation heat losses (ref. 12). From the individual stream properties, V, ρ and A, the properties of a hypothetical ideally-mixed stream were also calculated on a mass averaged basis.

Acoustic data reduction. - In order to convert the measured SPL's to the corresponding free-field values the assumption was made that for each frequency the jet can be treated as a pure harmonic point source at the center of the nozzle exit plane and that the impedance of the ground plane is infinite. Ground reflection corrections were then calculated for each microphone location and frequency (ref. 13) and applied to the measured spectral data (for each microphone). Corrections for atmospheric attenuation of the noise signal were added to the spectral data, using the information from reference 14 to obtain lossless data. A single spectrum for each measurement angle (from nozzle inlet) was obtained by combining the two sets of data obtained from the ground microphone and centerline microphone. The spectrum from the ground microphone was used over a frequency range from 100 to 1000 Hz and the spectrum from the centerline microphone was used over a frequency range

from 5000 Hz to 80K Hz. The data from both microphones were arithmetically averaged over the intermediate frequency range from 1250 to 4000 Hz.

Jet plume data reduction. - For each point, flow-field properties were calculated from the measured data. The measured pressures (total and static) were corrected for probe bow-shock effects, when necessary, according to reference 15. From these pressures the local Mach numbers were then calculated. Total temperature measurements were corrected for thermocouple radiation losses (ref. 12). Static temperatures were then computed from the Mach numbers and corrected total temperatures, and the local velocities were then calculated.

SOURCE LOCATION RESULTS

Experimental jet noise measurements are often made at a distance from the source great enough to be in the far field, but not far enough away to allow treatment of the entire noise generating region as a point source. Thus, the correlation of the noise from each region must take into account the location of that source region. The multiple-sideline noise measurements provide some useful information on the noise source distribution, as has been demonstrated for conical nozzles (e.g., ref. 16).

In order to determine source locations from multiple sideline noise data the following procedure was used:

(1) The directivity of each 1/3-octave-band is examined for each sideline, and the axial distance where the peak SPL occurs, X_{Pk}, is determined.

(2) Next, the nondimensionalized peak noise location, X_{Pk}/D_1, is plotted against frequency for each sideline, and curves are faired through the data for use in further computations.

(3) Finally, for each frequency X_{Pk}/D_1 is plotted against the dimensionless sideline distance, Y/D_1, and the results are linearly extrapolated to $Y/D_1 = 0$ (the jet axis); this intersection is the apparent source location X_s/D_1.

In the present tests, noise measurements were made at four sideline distances as illustrated in figure 4. The dimensionless axial position, X_{Pk}/D_1, of the maximum SPL in each 1/3 octave band is plotted versus frequency for each sideline in figure 7 for the inner nozzle operating alone as a conical nozzle at subsonic conditions (to avoid shock noise). This condition was repeated for each nozzle, so the repeatability of the results can be seen. The results for sideline-distance to inner-nozzle-diameter ratios, Y/D_1, of 17, 30, 50, and 70 are shown in figures 7(a) to (d), respectively. (The curves are faired as a series of lines in order to simplify calculations; the breaks from one slope to another have no significance.) The trends are quite reasonable with X_{Pk}/D_1 decreasing as frequency increases. It can also be seen that X_{Pk}/D_1

increases as Y/D_1 increases, indicating that each frequency peaks in the rear quadrant ($\theta > 90^{\circ}$).

Data such as those of figure 7 can be used to obtain approximate source locations for each frequency by plotting X_{Pk}/D_1 versus Y/D_1, and extrapolating to $Y/D_1 = 0$ to obtain X_s/D_1. Because of the relatively coarse microphone spacings and the data scatter, the faired curves of figure 7 are judged to be more suitable for this operation than the individual data points. Such plots are shown for several frequencies in figure 8. It can be seen that at frequencies above 10 kHz, the apparent X_s/D_1 is negative; this indicates the inadequacy of the present microphone spacings to resolve small X_s/D_1. It will be seen that the high frequencies corresponding to these small X_s/D_1 are well beyond the peak-SPL frequency in most cases.

The normalized source locations, X_s/D_1, are then plotted against Strouhal number fD_1/V_1, in figure 9. The results of reference 16 are also shown for comparison. For $X_s/D_1 \geq 4$ the present data agree reasonably well with the multiple-sideline results and the wall-isolation (shielding) results of reference 16. For further comparisons in this paper the solid faired curve, based on the present data for high X_s/D_1 and an extrapolation considering the data of reference 16 for small X_s/D_1, will be used.

Using the methods described above, source positions as a function of frequency were obtained for each nozzle configuration, and the results are shown in figure 10. Both streams were subsonic with $V_1 \cong 450$ m/sec and $V_2 \cong 570$ m/sec. No systematic trends with area ratio can be observed on this basis. In order to make more meaningful comparisons, the high frequency and low frequency data are plotted separately in figure 11. Because the low-frequency noise is thought to be generated in the merged region having a characteristic velocity, V_m, and a characteristic diameter D_m (e.g., ref. 6) X_s/D_m is plotted against fD_m/V_m (fig. 11(a)). Since the high frequency noise is thought to be generated by the outer stream relatively near the nozzle, the characteristic velocity is taken to be V_2 and the characteristic diameter is taken to be $2H_2$, the hydraulic diameter. Therefore, the high frequency data are plotted as $X_s/2H_2$ against $2fH_2/V_2$ in figure 11(b). In both cases the circular nozzle curve (solid curve of figure 9) is shown for reference. A data point for each configuration and each frequency is plotted in figure 11(a) or figure 11(b), not both. The data for both regimes show qualitative agreement with the circular nozzle curve, indicating the validity of the models for both regimes.

Rather than extrapolate each frequency from near-field to far-field, reference 6 made use of an approximate approach wherein the noise signal received at each far-field angle is related to a single source position corresponding to that of the peak-SPL frequency. In the present analysis, as in reference 6, this approach is applied separately to the merged and premerged regions. At each

microphone position on the furthest sideline ($Y/D_1 = 70$) the frequency at which the peak SPL occurs is determined and the corresponding peak-SPL Strouhal number is calculated. The peak-SPL Strouhal number as a function of angle is shown in figure 12(a) for the merged region and figure 13(a) for the premerged region. Each peak-SPL Strouhal number is also associated with a corresponding source location (from fig. 11) which is considered to be the source location for that angle. The corresponding normalized source locations are shown in figures 12(b) and 13(b). The simplified expressions of reference 6 for source position as a function of angle are shown for comparison. The difficulty in determining the low-frequency, merged-region spectral peaks is apparent in the scatter in figure 12(a), but the corresponding scatter in the source location (fig. 12(b)) is within the accuracy of the multiple-sideline source location technique. It is even more difficult to determine the high-frequency, premerged region spectral peaks (fig. 13(a)); this also results in greater scatter in the corresponding source location data (fig. 13(b)). Considering the data scatter, the predictions of reference 6 appear to be adequate. Further analysis may show that the prediction should be modified to give rear quadrant source positions farther downstream, but this would not have significant effect on the angle or source-to-observer distances for $Y/D_1 = 70$, where noise prediction comparisons will be made.

JET PLUME SURVEY RESULTS

An important aspect of this paper is the assessment of the methods by which the effective flow properties are determined for each noise generating region. Jet-plume surveys were made to provide the data needed in order to make such assessments.

Jet plume survey results for each configuration, which both streams subsonic ($V_1 = 450$ m/sec and $V_2 = 570$ m/sec) are shown in figure 14. The results for area ratios 1.2, 1.4, 1.9 and 3.2 are shown in figures 14(a) to (d), respectively. The local peak velocity and the local centerline velocity, both ratioed to the outer-stream ideal exit velocity, are plotted against X/D_1. The expected trends are shown most clearly in figure 14(c); the other plots are consistent with these but require some explanation. The peak velocity, which is initially in the outer-stream region, decreases rapidly with axial distance while the centerline velocity increases slightly; this type of behavior is associated with the premerged region and is consistent with the model of reference 6. With increasing area ratio, and therefore increasing flow in the outer stream, the length of the premerged region increases. For the smallest area ratio, the premerged region cannot be distinguished in the plume surveys, but this is probably because the first axial posi-

tion traversed is 5 inner-nozzle diameters downstream of the outer nozzle exit for that noncoplanar configuration.

At some distance downstream the centerline velocity reaches a maximum and begins to decrease. (Only fig. 14(c) shows this clearly, but results for other conditions also show this trend.) In about the same region or somewhat further downstream, the centerline velocity becomes the peak velocity; this vicinity and the region further downstream is termed the merged region. The merged region appears to start at X/D_1 from 1 to 10, depending on nozzle geometry, and extends to at least $X/D_1 = 15$ (from fig. 10). The flow properties within this region should characterize the low frequency noise generation. The low frequency noise of circular jets emanates from a region 4 to 8 diameters downstream, where the peak local velocity is from 0.8 to 0.95 that of the exit velocity. By analogy to the circular jet, the equivalent "exit" velocity of the merged region should be somewhat higher than the peak centerline velocity. The merged velocity, V_m, as suggested in reference 6, appears to be appropriate, with the peak centerline velocity ranging from 0.83 V_m to 0.92 V_m.

It appears that in general the flow property models of reference 6 are adequate for both the premerged region and the merged region.

COMPARISON OF NOISE PREDICTION WITH EXPERIMENTAL DATA

The NASA Lewis prediction method for inverted-velocity-profile jet noise, described in reference 6, is compared with several sets of experimental data. The preceding sections suggest that the assumptions made in formulating this prediction are reasonable. Comparisons were made in reference 6 with data for small area ratio (0.65 to 1.20) coaxial nozzles, and reasonable agreement was shown with both static (refs. 2 and 3) and simulated flight (ref. 17) data. Since this paper presents results for higher area ratios, the accuracy of the prediction can be tested over a wider range.

The first set of comparisons (figs. 15 to 18) includes all four nozzle geometries with both streams subsonic; these are the same conditions for which detailed source location and jet plume data are given in preceding sections. Spectral comparisons are shown for four angles, θ^*, in each case, 45°, 90°, 125° and 145°. Except at $\theta^* = 145^\circ$ the low frequency, merged region noise shows good agreement with the prediction. The problem at large angles and high jet velocities is believed to be due largely to inaccuracies in the empirical convection correlation (e.g., see ref. 18). Some of the experimental data exhibit anomalous trends at very high frequencies, which may be due to incorrect atmospheric absorption corrections and/or data system inadequacies. The premerged, high-frequency prediction appears to become less accurate

as the area ratio increases (or as radius ratio decreases). It appears that the premerged prediction may be too low by as much as 5 dB at the highest area ratio (fig. 18).

Tenative improvements have been identified which produce better agreement with the present data and have little effect on the comparisons shown in reference 6. The expressions used in the prediction of reference 6 are given in the Appendix A to this paper. The suggested modifications are as follows:

(1) The geometric and flow field effect given by eq. (A-1) should be replaced by

$$SPL_{P\ell} = SPL_j - 15 \log \left[1 + 1.5 \left(1 + \frac{V_1}{V_2} \right) \left(\frac{D_2 - 2H_2}{D_2} \right)^4 \right]$$

(2) The frequency shift term given in eq. (A-2) should be replaced by

$$f_p = f_j \sqrt{\frac{A_2}{\pi H_2^2}}$$

(3) The cutoff relation given by eq. (A-3) should be replaced by

$$SPL_p = SPL_{P\ell} - 10 \log \left[1 + \frac{V_2 \, (T_a/T_2)^{0.4}}{2fH_2 \, (1 + 0.2 \, L_2/H_2)} \right]$$

The results of the modified prediction are shown by the dashed curves in figures 15 to 18. The agreement in the middle and high frequency ranges is greatly improved. These changes in the prediction method should be considered preliminary, due to the limited comparisons made herein. These changes would influence the comparisons shown in reference 6 by 0.5 dB or less.

Having established the range of accuracy of the jet mixing noise prediction procedures, the next set of comparisons (figs. 19 and 20) includes outer-stream shock noise. The 1.4-area-ratio nozzle was operated at the same subsonic inner stream conditions as for the preceding figures, but with the outer stream at pressure ratios of 2.2 (fig. 19) and 3.0 (fig. 20). The shock noise is not as apparent in the experimental data as it is predicted to be, but the agreement between experimental data and prediction is better when shock noise is included. The need for further study of shock noise associated with inverted-velocity-profile coaxial nozzles is apparent.

CONCLUDING REMARKS

Experimental data are presented on the noise source distributions and flow field characteristics for inverted-velocity profile coaxial jets. The source location results were obtained from the analysis of multiple-sideline acoustic data. The flow field characteristics were determined from jet plume pressure/temperature traverses. The results obtained indicate that the flow field and source distribution relations incorporated in the NASA Lewis inverted velocity profile jet noise prediction procedure are reasonable. Comparisons of the prediction procedure with the present far-field acoustic data indicate that the procedure for merged region (low frequency) noise is also reasonable.

APPENDIX A

PREMERGED JET NOISE PREDICTION

This appendix is taken from reference 6 and briefly describes the premerged region prediction used therein.

The noise from the premerged-jet/ambient mixing region occurs at intermediate to high frequencies. Though it is usually less important that the merged noise for the full-scale case statically, in flight its importance may be enhanced, particularly with regard to the PNL. The method of prediction, illustrated conceptually in figure 21, is to treat the outer stream as if it were exhausting from a plug nozzle. However, the low frequency region is attenuated (shaded region labeled "cut-off" in fig. 21) since the outer jet decays rapidly with downstream axial distance, before much low frequency noise is generated. The same circular jet noise prediction (ref. 9) is used as a starting point here as was used for the merged jet, but both frequency and [illegible] shifts are made to account for plug nozzle effects and interaction of the two streams.

Plug nozzle and interaction effects. - Plug nozzles have been found to produce somewhat less noise than circular nozzles of the same area, and such an effect was included in reference 6. More recent results (e.g., ref. 3) have indicated a stronger plug effect, and the presence of inner stream flow also has an effect, so a new relationship is needed. The following relationship, based on a modification to the reference 9 plug nozzle effect, is used in reference 6*:

$$SPL_{Pl} = SPL_j + 5 \log \left[0.1 + 2\left(\frac{H_2}{D_2}\right)\left(1 - \frac{V_1}{V_2}\right) + 2\left(\frac{H_2 + H_1}{D_2}\right) \frac{(V_1/V_2)^{20}}{1 + (V_1/V_2)^{20}} \right] \tag{A-1}$$

(The term incorporating velocity ratio the twentieth power brings about approximately correct limiting behavior, recalling that the present method is limited to $V_2 > V_1$.) The plug nozzle noise is also shifted to higher frequency than the equivalent circular nozzle; the relationship of reference 9 is used for this effect,

*There is a typographical error in this equation in reference 6; the first term inside the brackets should be 0.1 not 1.

$$f_p = f_j \left(\frac{A_2}{\pi H_2^2} \right)^{0.2} \qquad \text{(A-2)}$$

Cut-off. - To account for the fact that the annular outer jet loses its identity before much noise is generated at low frequency, the following correction is applied:

$$SPL_p = SPL_{P\ell} - 10 \log \left[1 + \frac{V_2}{f(2H_2 + L_2)} \left(\frac{T_a}{T_2} \right)^{0.4} \right] \qquad \text{(A-3)}$$

APPENDIX B

SYMBOLS

A	nozzle exit area
D	inner diameter
f	1/3-octave-band center frequency
H	gap height (radius for circular nozzle)
L_2	spacing of inner nozzle exit plane downstream of outer nozzle exit plane
SPL	1/3-octave-band sound pressure level, dB re 20 $\mu N/m^2$
T	total temperature (absolute)
V	velocity
X	distance downstream from inner nozzle exit plane
Y	perpendicular distance from nozzle axis
θ	noise emission angle (relative to nozzle inlet axis)
θ^*	microphone angle (referred to arbitrary source array, (fig. 4)
ρ	density

Subscripts:

a	ambient
j	circular jet
m	merged region
1	inner stream
2	outer stream
Pk	peak
Pl	plug nozzle
p	premerged
S	source

REFERENCES

1. Willis, E., "Variable-Cycle Engines for Supersonic Cruise Aircraft," Variable Geometry and Multicycle Engines, AGARD CP-205, 1976, pp. 7-1 to 7-19.

2. Kozlowski, H., and Packman, A. B., "Aerodynamic and Acoustic Tests of Duct-Burning Turbofan Exhaust Nozzle," NASA CR-2628, 1976.

3. Knott, P. R., Stringas, E. J., Brausch, J. F., Staid, P. S., Heck, P. H., and Latham, D., "Acoustic Tests of Duct-Burning Turbofan Jet Noise Simulation," NASA CR-2966, 1978.

4. Gutierrez, O. A., "Aeroacoustic Studies of Coannular Nozzles Suitable for Supersonic Cruise Aircraft Applications," Proceedings of the SCAR Conference, Part 2. NASA CP-001, 1976, pp. 471-490.

5. Packman, A. B., Kozlowski, H., and Gutierrez, O., "Jet Noise Characteristics of Unsuppressed Duct-Burning Turbofan Exhaust System," Journal of Aircraft, Vol. 14, no. 3, 1977, pp. 227-232.

6. Stone, J. R., "An Empirical Model for Inverted-Velocity-Profile Jet Noise Prediction," NASA TM-73838, 1977.

7. Pao, S. P., "A Correlation of Mixing Noise from Coannular Jets with Inverted Flow Profiles," NASA TP-1301, 1979.

8. Larson, R. S., "A Jet Exhaust Noise Prediction Procedure for Inverted Velocity Profile Coannular Nozzles," AIAA Paper 79-0633, Mar. 1979.

9. Stone, J. R., "Interim Prediction Method for Jet Noise," NASA TM X-71618, 1974.

10. Harper-Bourne, M. and Fisher, M. J., "The Noise from Shock Waves in Supersonic Jets," Noise Mechanisms, AGARD-CP-131, 1973, pp. 11-1 to 11-13.

11. Goodykoontz, J. H. and Stone, J. R., "Experimental Study of Coaxial Nozzle Exhaust Noise," AIAA Paper 79-0631, Mar. 1979.

12. Glawe, G. E., Simmons, F. S., and Stickney, T. M., "Radiation and Recovery Corrections and Time Constants of Several Chromel-Alumel Thermocouple Probes in High-Temperature, High-Velocity Gas Streams," NACA TN-3766, 1956.

13. Howes, W. L., "Ground Reflection of Jet Noise," NASA TR R-35, 1959.

14. Shields, F. D. and Bass, H. E., "Atmospheric Absorption of High Frequency Noise and Application to Fractional Octave Bands," NASA CR-2760, 1977.

15. "Equations, Tables, and Charts for Compressible Flow," NACA Report 1135, 1953.

16. Jaeck, C. L., "Static and Wind Tunnel Near-Field/Far-Field Jet Noise Measurements from Model Scale Single-Flow Baseline and Suppressor Nozzles. Vol. I: Noise Source Locations and Extrapolation of Static Free-Field Jet Noise Data," NASA CR-137913, 1976.

17. Kozlowski, H. and Packman, A. B., "Flight Effects on the Aerodynamic and Acoustic Characteristics of Inverted-Profile Coannular Nozzles," NASA CR-3018, 1978.

18. Stone, J. R., "One the Use of Relative Velocity Exponents for Jet Engine Exhaust Noise," NASA TM-78873, 1978.

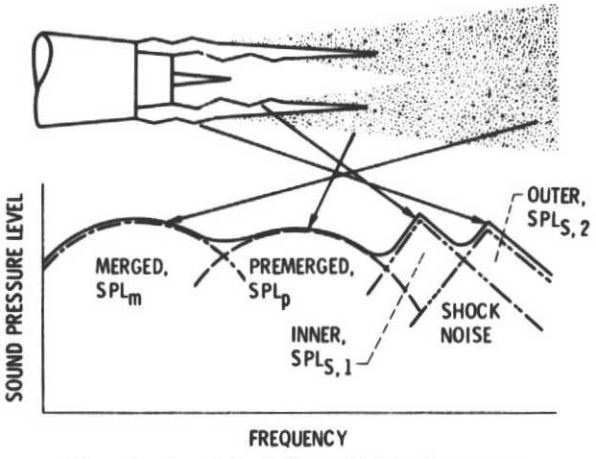

Figure 1. - Inverted-velocity-profile jet noise sources.

ORIGINAL PAGE IS
OF POOR QUALITY

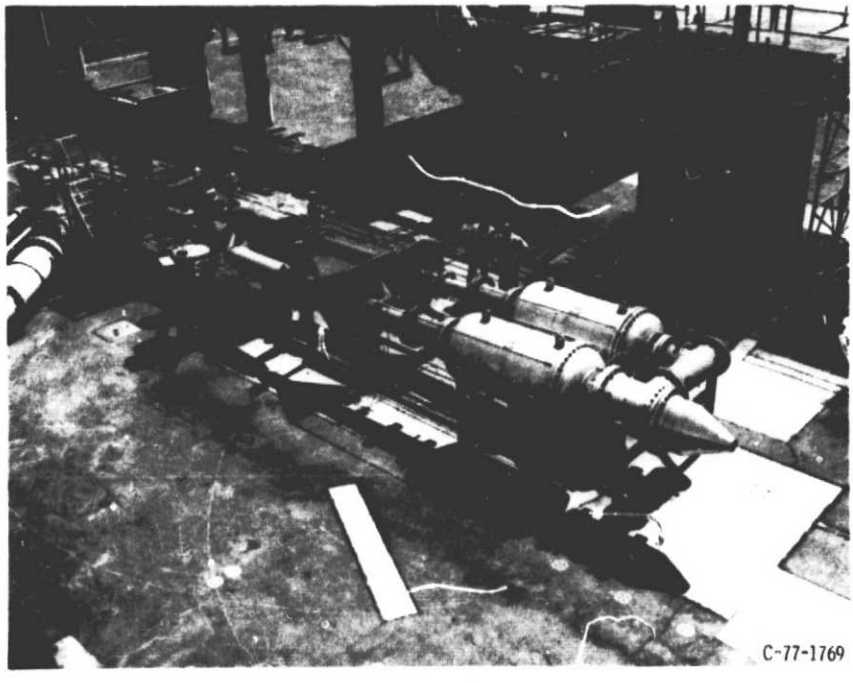

Figure 2. - Coaxial nozzle flow facility.

NOZZLE AREA RATIO	OUTER STREAM RADIUS RATIO*	D_1, cm	D_2, cm	H_2, cm	L_2, cm
1.2	0.95	10.0	36.10	0.90	40.6
1.4	.68	↓	15.98	2.56	0
1.9	.62		17.60	3.34	↓
3.2	.52		20.96	5.03	

*$\frac{D_2 - 2H_2}{D_2}$

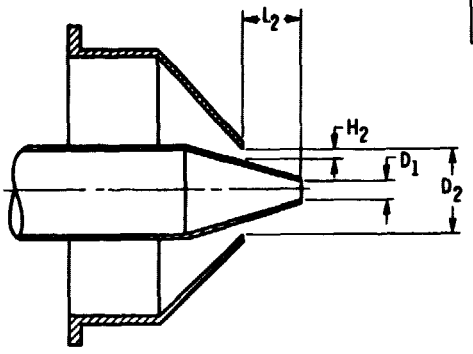

Figure 3. - Schematic of experimental coaxial nozzles.

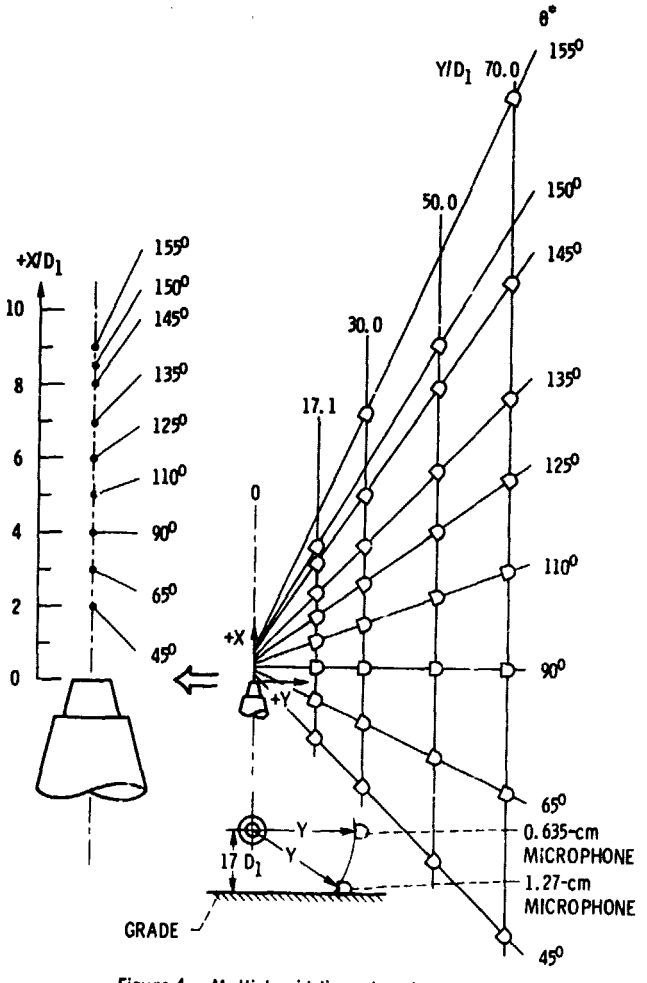

Figure 4. - Multiple-sideline microphone arrays.

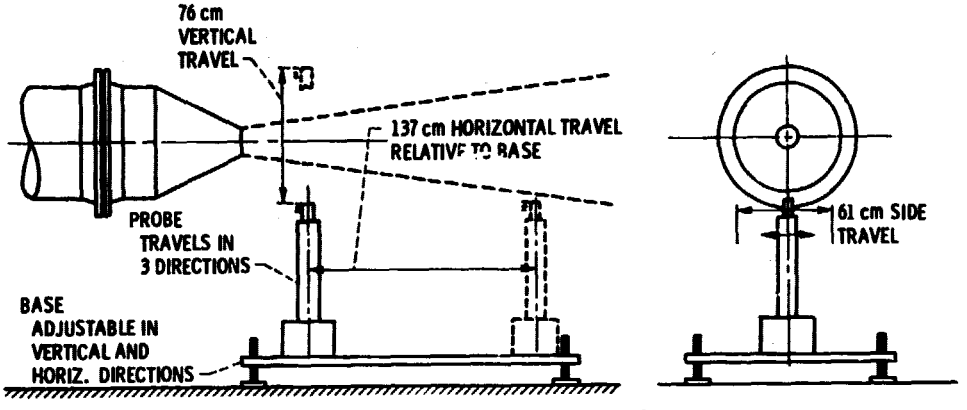

Figure 5. - Jet plume survey arrangement.

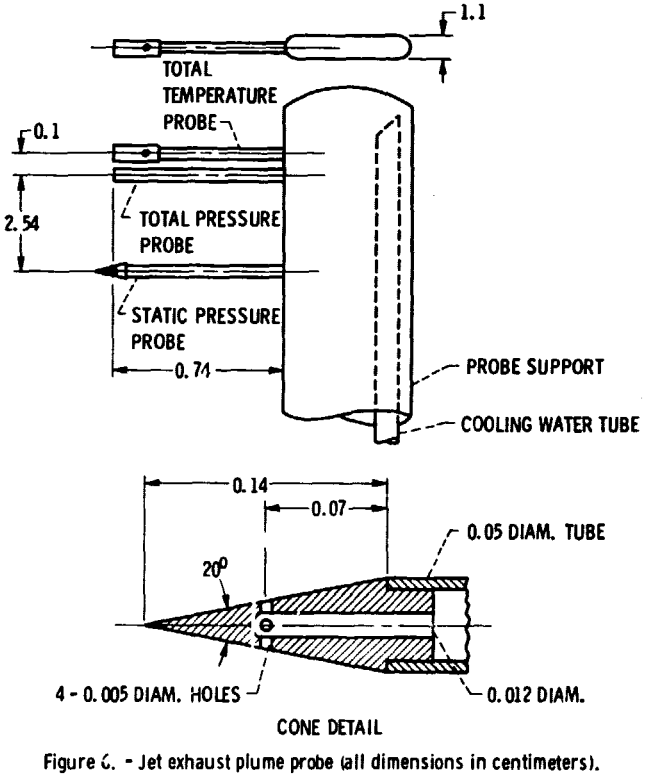

Figure 6. - Jet exhaust plume probe (all dimensions in centimeters).

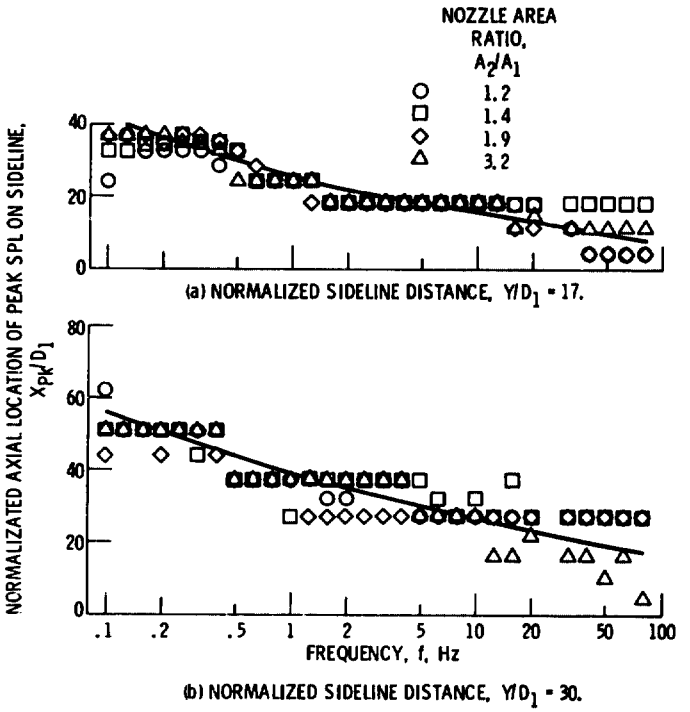

(a) NORMALIZED SIDELINE DISTANCE, $Y/D_1 = 17$.

(b) NORMALIZED SIDELINE DISTANCE, $Y/D_1 = 30$.

Figure 7. - Peak-SPL location as a function of frequency for conical nozzle (no flow in outer stream) for various sidelines; subsonic flow, $V_1 \approx 590$ m/sec.

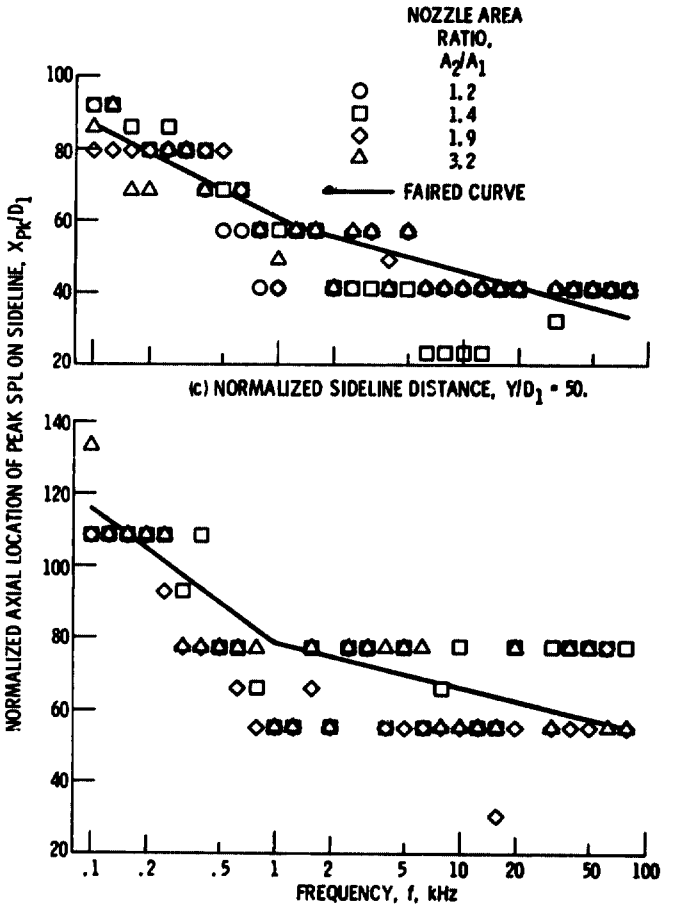

(c) NORMALIZED SIDELINE DISTANCE, $Y/D_1 = 50$.

(d) NORMALIZED SIDELINE DISTANCE, $Y/D_1 = 70$.

Figure 7. - Concluded.

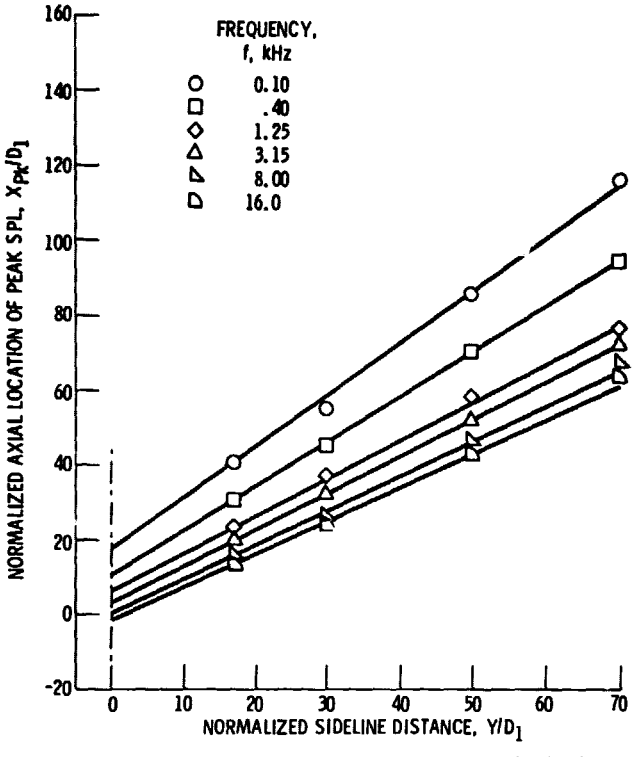

Figure 8. - Multiple-sideline source location determination for conical nozzle, subsonic flow, $V_1 \approx 590$ m/sec.

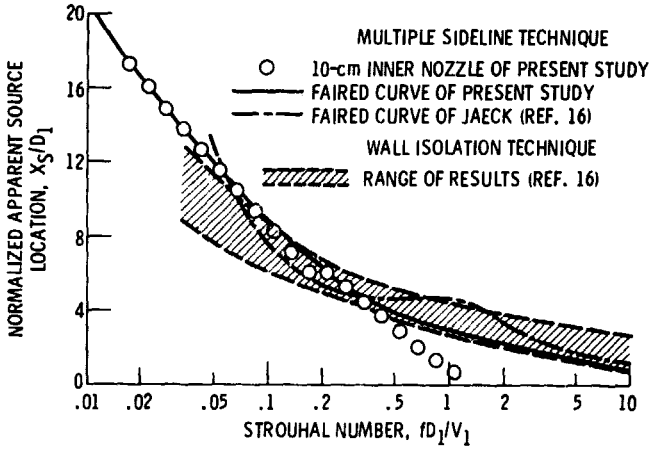

Figure 9. - Normalized apparent source location as a function of Strouhal number for conical nozzles.

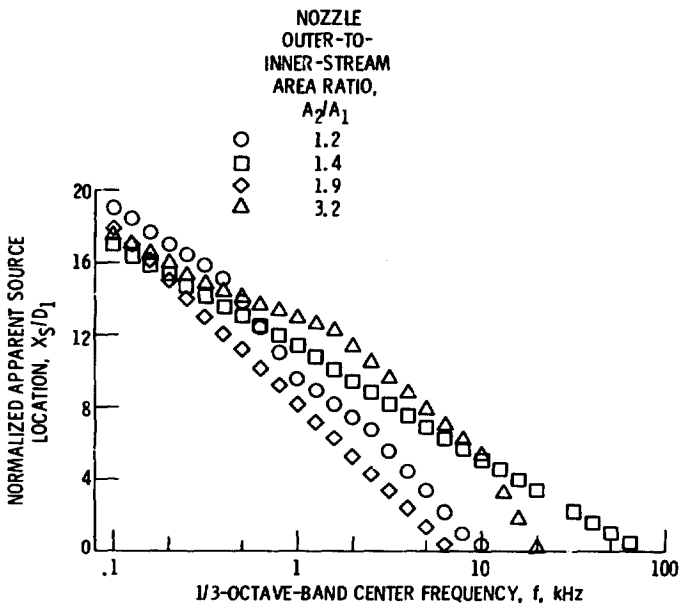

Figure 10. - Normalized apparent source location as a function of frequency for inverted-velocity-profile coaxial nozzles with both streams subsonic.

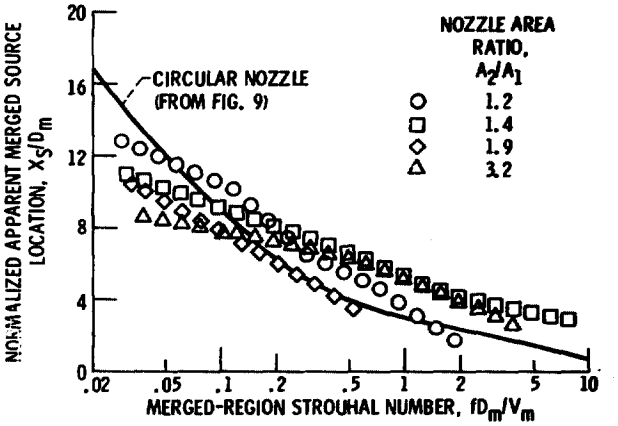

(a) MERGED REGION.

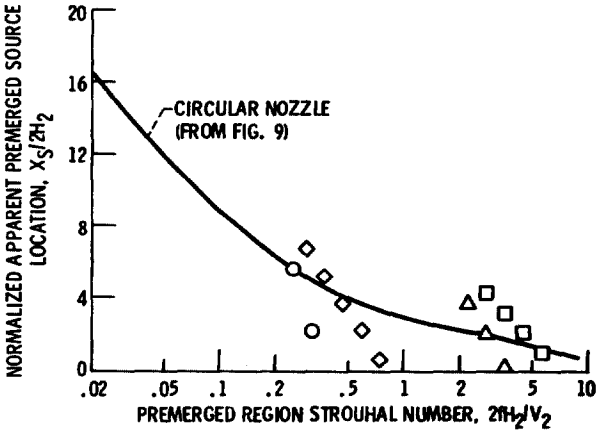

(b) PREMERGED REGION.

Figure 11. - Individual region normalized source locations as a function of appropriate Strouhal numbers for inverted velocity-profile coaxial nozzles with both streams subsonic.

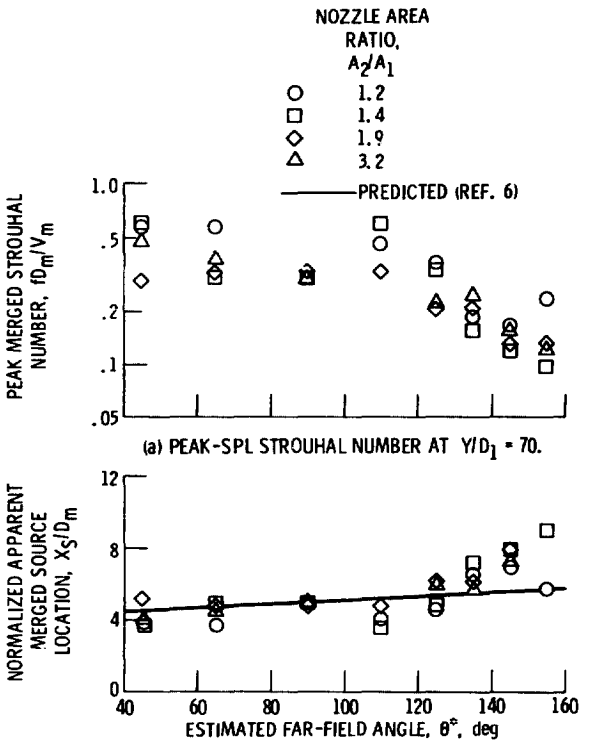

Figure 12. - Peak-SPL Strouhal number and corresponding source locations as a function of angle for merged region.

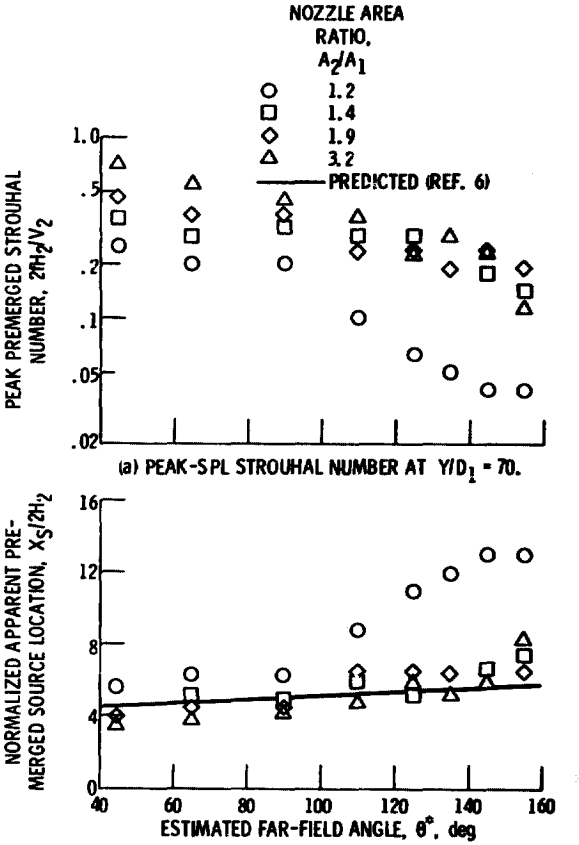

Figure 13. - Peak-SPL Strouhal number and corresponding source locations as a function of angle for premerged region.

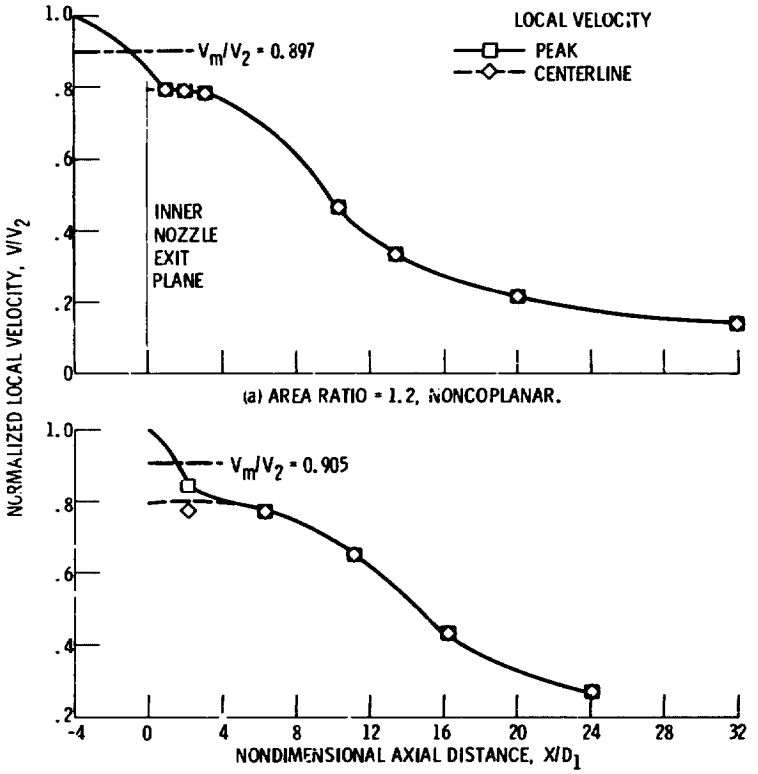

Figure 14. - Peak and centerline axial velocity decay for inverted-velocity-profile coaxial nozzle with both streams subsonic.

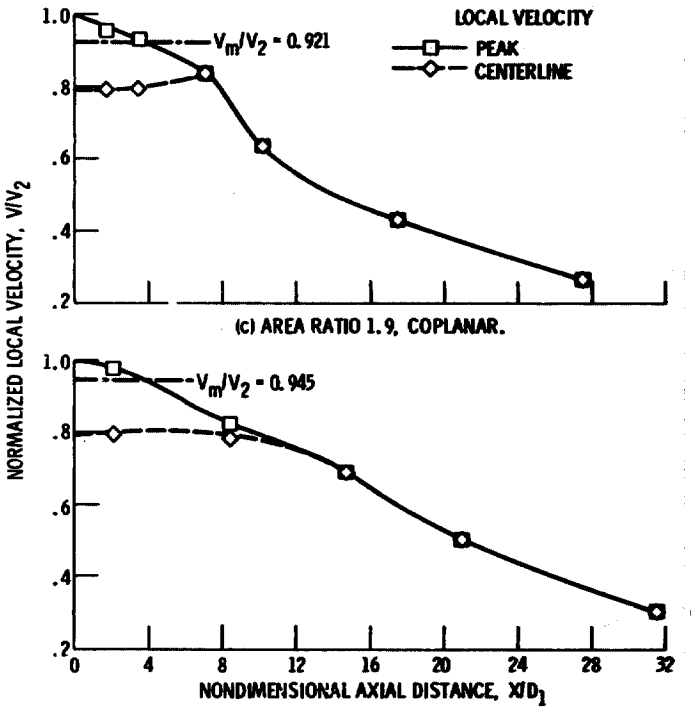

Figure 14. - Concluded.

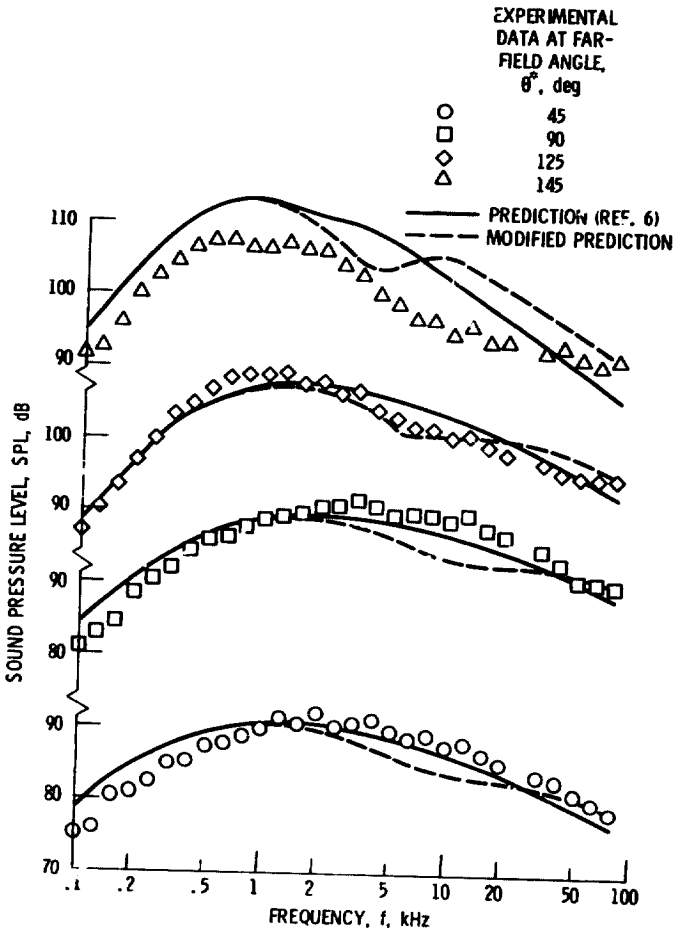

Figure 15. - Comparison of experimental and predicted spectra for 1.2-area-ratio noncoplanar coaxial nozzle with both streams subsonic. Outer-stream velocity 562 m/sec and temperature 1062 K; inner-stream velocity 448 m/sec and temperature 813 K.

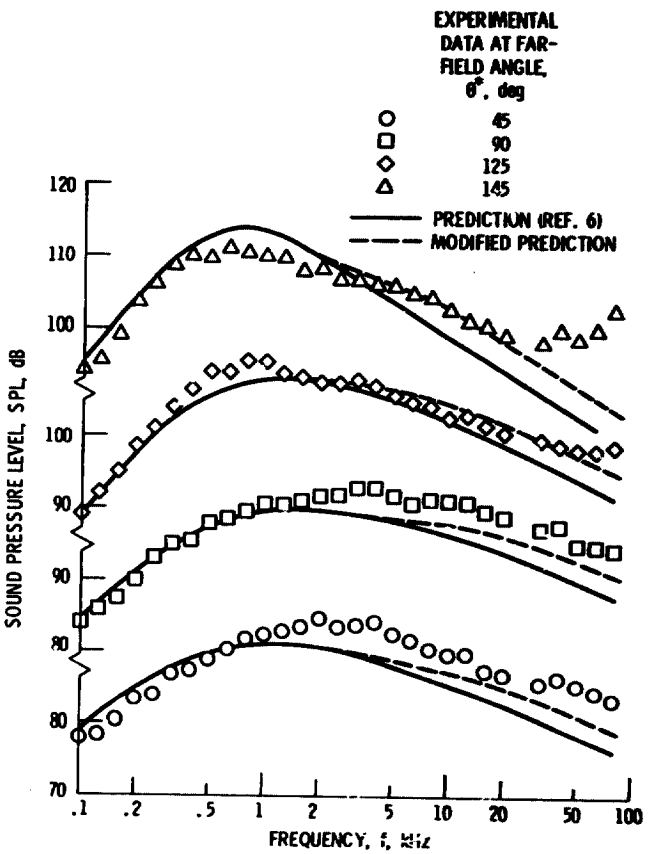

Figure 16. - Comparison of experimental and predicted spectra for 1.4-area-ratio coplanar coaxial nozzle with both streams subsonic. Outer stream velocity 574 m/sec and temperature 1063 K; inner stream velocity 460 m/sec and temperature 813 K.

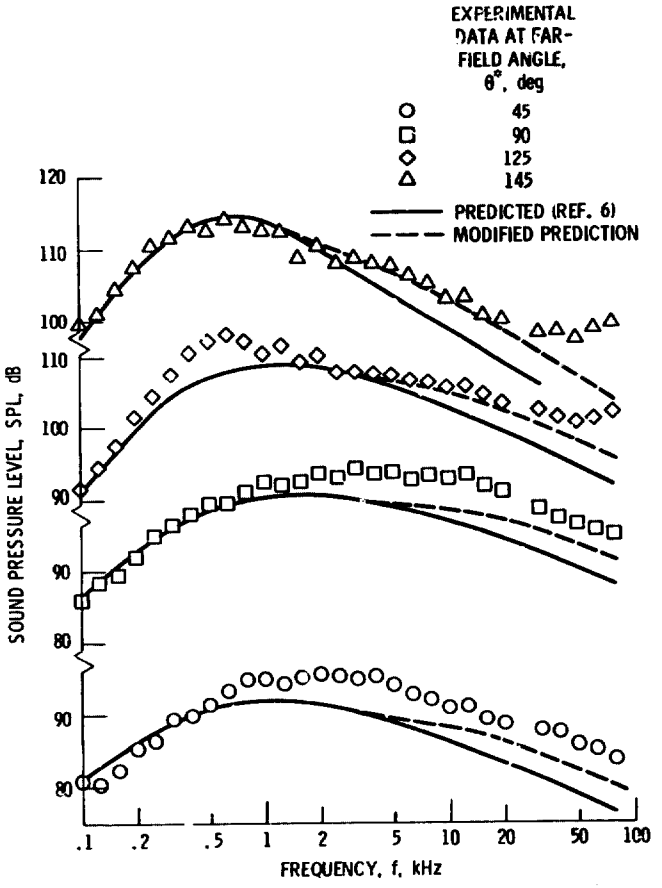

Figure 17. - Comparison of experimental and predicted spectra for 1.9-area-ratio coplanar coaxial nozzle with both streams subsonic. Outer-stream velocity 568 m/sec and temperature 1070 K; inner-stream velocity 446 m/sec and temperature 812 K.

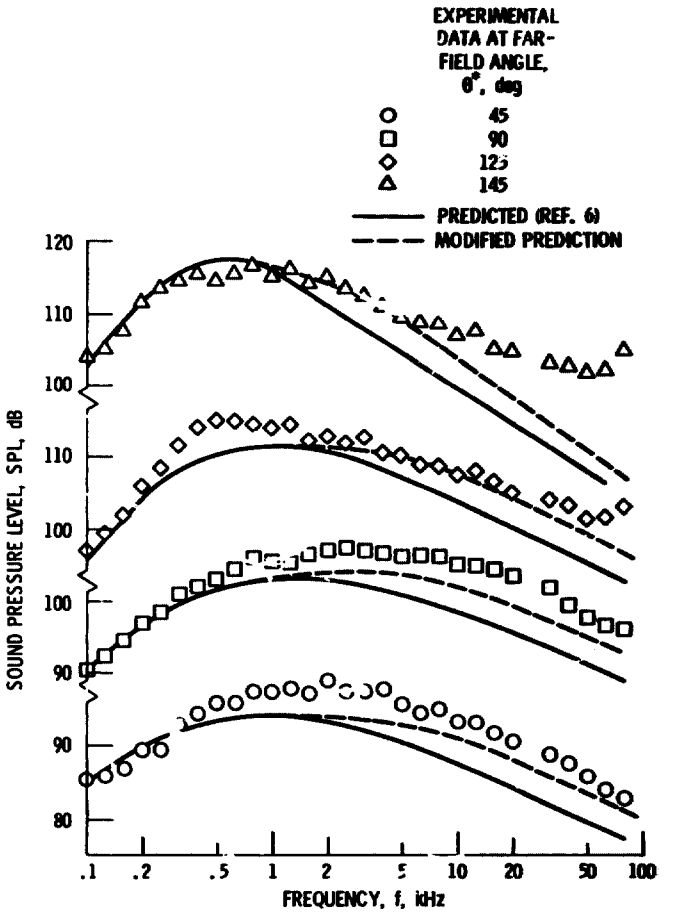

Figure 18. - Comparison of experimental and predicted spectra for 3.2-area-ratio coplanar coaxial nozzle with both streams subsonic. Outer-stream velocity 568 m/sec and temperature 1075 K; inner-stream velocity 445 m/sec and temperature 808 K.

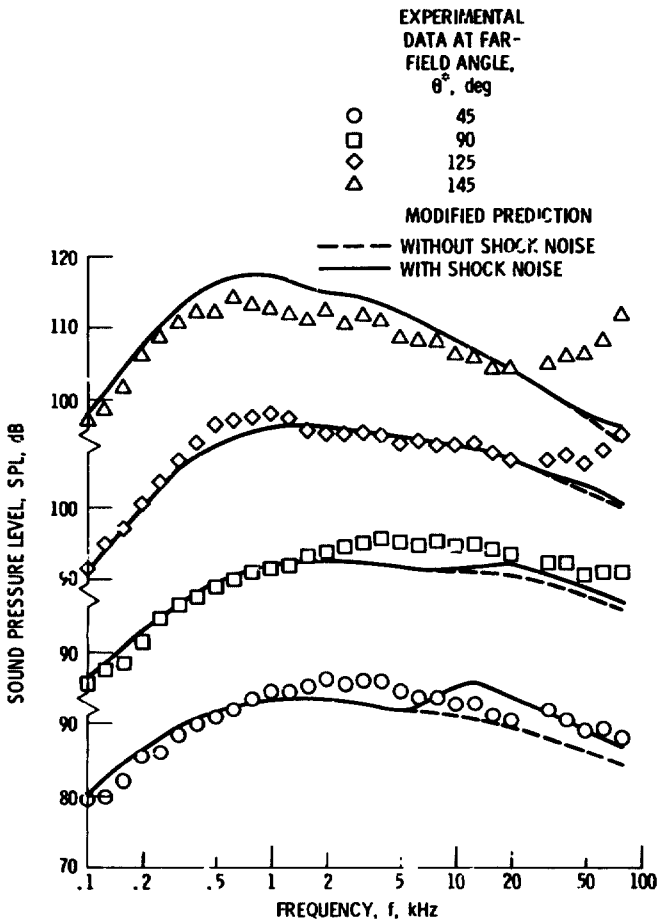

Figure 19. - Comparison of experimental and predicted spectra for 1.4-area-ratio coplanar coaxial nozzle with inner stream subsonic and outer stream supersonic. Outer-stream velocity 663 m/sec and temperature 1073 K; inner-stream velocity 460 m/sec and temperature 812 K.

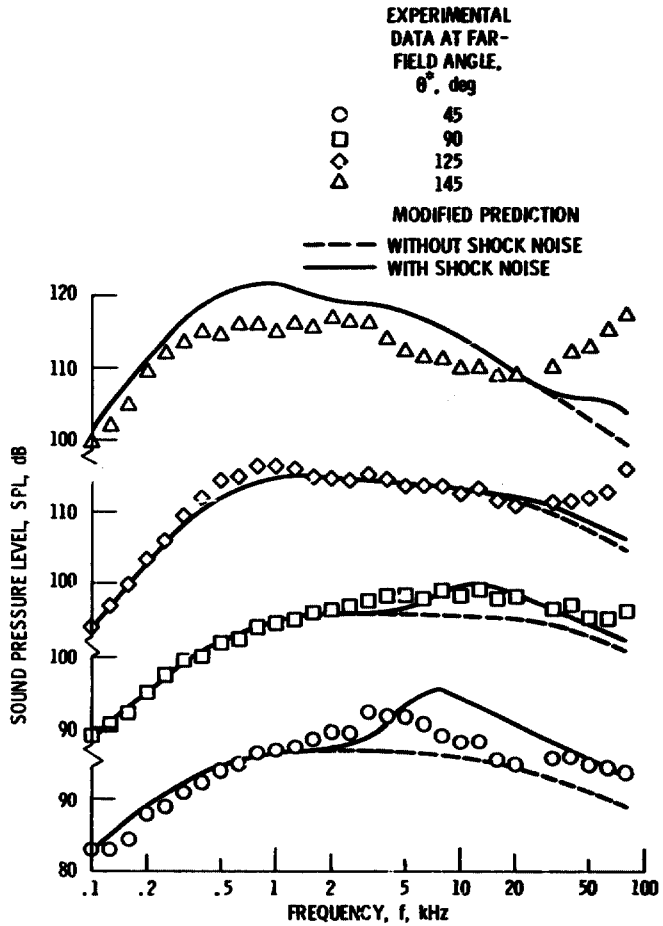

Figure 20. - Comparison of experimental and predicted spectra for 1.4-area-ratio coplanar nozzle with inner-stream subsonic and outer-stream supersonic. Outer-stream velocity 765 m/sec and temperature 1067 K; inner-stream velocity 458 m/sec and temperature 811 K.

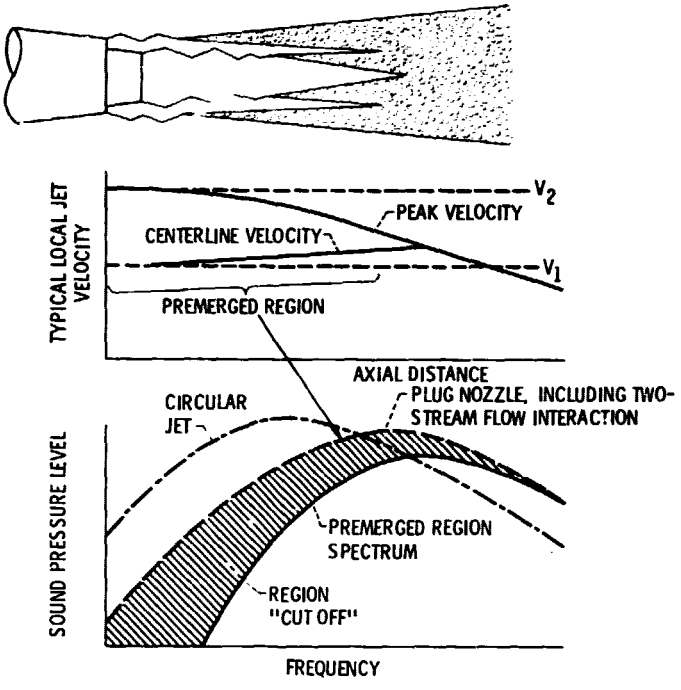

Figure 21. - Modeling of premerged, high-frequency region noise generation for an inverted-velocity-profile coaxial jet.